



The impact of RS80  
bias

Y. Inai et al.

This discussion paper is/has been under review for the journal Atmospheric Measurement Techniques (AMT). Please refer to the corresponding final paper in AMT if available.

# Altitude misestimation caused by the Vaisala RS80 pressure bias and its impact on meteorological profiles

Y. Inai<sup>1</sup>, M. Shiotani<sup>1</sup>, M. Fujiwara<sup>2</sup>, F. Hasebe<sup>2</sup>, and H. Vömel<sup>3</sup>

<sup>1</sup>Research Institute for Sustainable Humanosphere, Kyoto University, Uji, Japan

<sup>2</sup>Faculty of Environmental Earth Science, Hokkaido University, Sapporo, Japan

<sup>3</sup>Earth Observing Laboratory, The National Center for Atmospheric Research, Boulder, USA

Received: 4 February 2015 – Accepted: 5 February 2015 – Published: 25 February 2015

Correspondence to: Y. Inai (yoichi\_inai@rish.kyoto-u.ac.jp)

Published by Copernicus Publications on behalf of the European Geosciences Union.

Title Page

Abstract

Introduction

Conclusions

References

Tables

Figures



Back

Close

Full Screen / Esc

Printer-friendly Version

Interactive Discussion



## Abstract

Previous research has found that conventional radiosondes containing a traditional pressure sensor can be subject to a pressure bias, particularly in the stratosphere. This study examines this pressure bias, and the resulting altitude misestimation, and considers its impact on temperature, ozone, and water vapor profiles, using data obtained between December 2003 and January 2010 during the Soundings of Ozone and Water in the Equatorial Region (SOWER) campaigns. The observation package consisted of a radiosonde (Vaisala RS80), ozone and water vapor sondes, and a global positioning system (GPS) sensor. More than 30 soundings are used in this study. As GPS height data are thought to be highly accurate, they can be used to calculate pressure. The RS80 pressure bias in the tropical stratosphere was estimated to be  $-0.4 \pm 0.2$  hPa ( $1\sigma$ ) between 20 and 30 km. As this pressure bias is negative throughout the stratosphere, it leads to altitude misestimation when heights are calculated, as this is usually achieved using the hydrostatics equation. We estimated the error in geometric height to be  $42 \pm 24$ ,  $110 \pm 39$ , and  $240 \pm 90$  m ( $1\sigma$ ) at 20, 25, and 30 km, respectively. Because of the altitude misestimation, we saw some differences in observation parameters having a vertical gradient. For the temperature profiles, the differences were approximately  $-0.2 \pm 0.2$ ,  $-0.2 \pm 0.4$ , and  $-0.3 \pm 0.8$  K ( $1\sigma$ ) at 20, 25, and 30 km, respectively. For the ozone profiles, there was a maximum of ozone partial pressure at around 27 km. Therefore, the differences do not monotonically increase with increasing altitude, and they are estimated to be  $-1.9 \pm 1.6$ ,  $-0.7 \pm 1.0$ , and  $3.1 \pm 2.2$  % ( $1\sigma$ ) at 20, 25, and 30 km, respectively. For the water vapor profiles, as there are minima and maxima associated with the stratospheric tape recorder signal, the differences are affected by the phase of the tape recorder. If we align water vapor profiles using a water vapor minimum, the differences are estimated to be  $-2.7 \pm 8.1$  % at 0.5 km and  $1.5 \pm 1.0$  % ( $1\sigma$ ) at 4 km above the water vapor minimum around the cold point tropopause. These biases in the meteorological soundings obtained using the RS80 may have generated an artificial trend in the meteorological records when radiosondes were changed from

## AMTD

8, 2191–2222, 2015

### The impact of RS80 bias

Y. Inai et al.

Title Page

Abstract

Introduction

Conclusions

References

Tables

Figures



Back

Close

Full Screen / Esc

Printer-friendly Version

Interactive Discussion



the RS80, which had no GPS sensor, to the new ones with a GPS sensor. Therefore, it is important to take these biases into account in climate change studies.

## 1 Introduction

Radiosondes are one of the most important observation tools used in meteorological studies to measure in situ temperature, pressure, humidity, and horizontal wind above the surface up to around 30 km. There are many vendors supplying radiosondes for operational and scientific observations, and extensive intercomparisons have been conducted (Nash and Schmidlin, 1987; Nash et al., 2006, 2011; Ivanov et al., 1991; Yagi et al., 1996; da Silveira et al., 2006).

Traditionally, the hypsometric equation has been used to calculate height information from pressure, temperature, and humidity measurements. Currently, however, global positioning system (GPS) technology is used for altitude derivation, and pressure is inversely derived from the GPS height data (Jannet et al., 2008). Over the past decade, the old-type radiosondes, which have no GPS receiver, have been replaced by new-type radiosondes with a GPS receiver.

The Vaisala RS80 radiosonde has been used worldwide since 1981, and their market share was 48 % of all radiosonde stations globally as of March 2002 (Elms, 2003). Recently, it has been reported that the RS80 radiosonde shows a negative pressure bias in the stratosphere (e.g., Steinbrecht et al., 2008; Inai et al., 2009). Such a negative pressure bias could cause height overestimation; i.e., estimated heights being greater than the actual height. Moreover, this results in a negative temperature bias at a given altitude in the stratosphere, where temperature increases with increasing height. Steinbrecht et al. (2008) suggested that this RS80 negative pressure bias, together with the changeover to the Vaisala RS92, which is an updated version of the RS80, could lead to a discontinuity in the stratospheric temperature record.

Many studies have reported that the stratospheric temperature shows a long-term cooling trend (e.g., Randel and Wu, 2006; Randel et al., 2009), although a warming

## The impact of RS80 bias

Y. Inai et al.

Title Page

Abstract

Introduction

Conclusions

References

Tables

Figures



Back

Close

Full Screen / Esc

Printer-friendly Version

Interactive Discussion



## The impact of RS80 bias

Y. Inai et al.

Title Page

Abstract

Introduction

Conclusions

References

Tables

Figures



Back

Close

Full Screen / Esc

Printer-friendly Version

Interactive Discussion



trend has been reported in the tropical upper troposphere and lower stratosphere during the 21st century (Ladstädter et al., 2011). In such a sensitive area for trend analysis, historical temperature records from radiosonde observations should be used with care. It has also been shown that tropical lower stratospheric ozone levels follow a negative trend (Randel and Thompson, 2011). Ozonesonde data have been widely used for such ozone trend analysis, but again, we must be wary of the possible pressure bias, because an ozonesonde is usually equipped with a radiosonde for measuring temperature, pressure, and humidity.

Stauffer et al. (2014) discussed possible errors in ozone profiles caused by pressure biases from various types of conventional radiosondes, including the RS80. They pointed out that these pressure biases can produce observational errors when estimating the ozone mixing ratio using biased pressure information. The pressure bias of the RS80 is larger than that of the RS92, but similar to that of the International Met Systems (iMet) series in their study.

Stauffer et al. (2014) used data taken from the observation package of a radiosonde and an ozonesonde with a GPS sensor, and recalculated ozone mixing ratios by replacing observed (biased) pressure with corrected (unbiased) pressure. It would be useful if we were able to use GPS height data as a proper vertical coordinate to assign to measurements from a radiosonde and an ozonesonde. However, in the typical situation where no GPS sensor is available, we must calculate height information using the hydrostatic equation. The observed profiles should then be moved vertically according to the altitude offset, resulting in quantitative errors if observed parameters have a vertical gradient. Therefore, the approach of Stauffer et al. (2014) is insufficient to assess the impact of radiosonde pressure bias on meteorological datasets.

In this study, we show the impact of the vertical shift on observed temperature profiles (in Sect. 4.1), ozone profiles (in Sect. 4.2), and water vapor profiles (in Sect. 4.3) based on measurements made with an RS80 radiosonde, as well as water vapor and ozone sondes with a GPS sensor, obtained during the Soundings of Ozone and Water in the Equatorial Region (SOWER) campaigns.

## 2 SOWER data

The SOWER campaigns in the tropical western Pacific/Indonesian region have been conducted in every boreal winter since December 2001 to study processes in the tropical tropopause layer (TTL) (e.g., Fujiwara et al., 2010; Inai et al., 2012, 2013; Shibata et al., 2012; Hasebe et al., 2013). During the SOWER campaigns, 33 successful soundings were conducted with the combined use of an RS80 radiosonde, an electrochemical concentration cells (ECC) ozonesonde together with a GPS sensor, and a chilled-mirror hygrometer, from December 2003 to January 2010. All of the GPS sensors were provided by the Garmin Ltd. and situated in the lid of the Environmental Science Corporation (En-Sci) ECC ozonesondes. These data are used in this study (Table 1). We estimate the RS80 pressure bias using these data following the method of Inai et al. (2009), and thus examine how the RS80 pressure bias affects profiles of meteorological parameters such as temperature, ozone, and water vapor. A preliminary consideration of this issue was briefly reported in Imai et al. (2013), but in this paper we present our viewpoint and approach in detail.

Note that the SOWER data were not obtained using the genuine Vaisala system, which automatically corrects pressure data with an independent ground-based barometer, and the SOWER data used in this paper were consolidated according to our quality control (QC) procedure to ensure their uniformity. These data have also been used in previous studies such as Inai et al. (2009) and Imai et al. (2013); the QC procedure is summarized in the Appendix. We also compare our results with those of Stauffer et al. (2014).

## 3 RS80 pressure bias

Whereas a GPS sensor reports an altitude above the WGS-84 ellipsoid (NIMA, 2000) (GPS altitude  $\equiv Z_{\text{GPS}}$ ), the geometric altitude ( $z$ ) is defined by the absolute altitude above mean sea level (a.m.s.l.). In this study, we obtained the geometric altitudes from

AMTD

8, 2191–2222, 2015

## The impact of RS80 bias

Y. Inai et al.

Title Page

Abstract

Introduction

Conclusions

References

Tables

Figures



Back

Close

Full Screen / Esc

Printer-friendly Version

Interactive Discussion



$z_{\text{GPS}}$  by using the station altitude a.m.s.l. as the initial GPS altitude. Thus, the precision of  $z$  is the same as that of  $z_{\text{GPS}}$ , and is accurate to within approximately 20 m between the surface and a height of 34 km (Nash et al., 2006). In the following, we use  $z$  values obtained from the GPS as a reference vertical coordinate.

Alternatively, using vertical profile data for pressure ( $p$  [ $\text{N m}^{-2}$ ]), temperature ( $T$  [K]), and humidity ( $U$  in percent), we can obtain the approximate geometric altitude,  $z_{\text{PTU}}$ , by integrating the hydrostatics equation (e.g., Holton, 2004):

$$z_{\text{PTU}}(p) = - \int_{p_0}^p \frac{R^* T}{g M_d} \frac{1}{p' + \frac{U}{100} \rho_{\text{ws}} \left( \frac{M_w - M_d}{M_d} \right)} dp' + z_0. \quad (1)$$

Here,  $R^*$  is the universal gas constant ( $8314.51 \text{ [JK}^{-1} \text{ kmol}^{-1}]$ ),  $M_d$  is the molecular weight of dry air ( $28.96 \text{ [kg kmol}^{-1}]$ ),  $M_w$  is that of water vapor ( $18.015 \text{ [kg kmol}^{-1}]$ ),  $\rho_{\text{ws}}$  is the saturation water vapor partial pressure [ $\text{N m}^{-2}$ ] from  $T$ , and  $p_0$  and  $z_0$  are the pressure and geometric altitude a.m.s.l. at the first step of the integration, respectively. The gravity field  $g$  depends on latitude and altitude (e.g., NIMA, 2000), and in Eq. (1) we use the same equations as Stauffer et al. (2014) to allow consistent comparisons. As  $z_{\text{PTU}}$  is calculated from PTU, the precision and accuracy depend on those of the pressure, temperature, and humidity sensors. Inai et al. (2009) showed that among these parameters, the accuracy of the pressure sensor is essential in the stratosphere. Note that we use geometric height, not geopotential height, throughout this study, but those geometric altitudes  $z$  and  $z_{\text{PTU}}$  can be converted to geopotential altitudes, respectively (e.g., Mahoney, 2005), which is conventionally used in meteorological studies.

Figure 1 shows the differences between  $z_{\text{PTU}}$  and  $z$  at the same observation time for all soundings listed in Table 1. Although the difference is small ( $\sim 20$  m) in the troposphere, it becomes larger in the stratosphere with a difference of  $\sim 240$  m at 30 km on average. A similar bias of  $z_{\text{PTU}}$  was reported and discussed by Inai et al. (2009). In the present analysis, the data period was extended to include the 2010 campaign, but data from Hanoi located in the subtropics, were excluded because we now have sufficient

## The impact of RS80 bias

Y. Inai et al.

Title Page

Abstract

Introduction

Conclusions

References

Tables

Figures



Back

Close

Full Screen / Esc

Printer-friendly Version

Interactive Discussion



sounding data even from the tropics. The following section shows a typical example of sounding profile (BI048), which is highlighted by a red line in Fig. 1.

In recent years, almost all radiosonde systems have used GPS height information together with temperature and humidity to derive pressure ( $p_{\text{GPS}}$ ). In this study, we calculate  $p_{\text{GPS}}$  based on the following equation:

$$d \ln p_{\text{GPS}} = \frac{-gM_d}{R*T \left( 1 - \frac{u}{100} \frac{\rho_{\text{ws}}}{\rho} \frac{M_w - M_d}{M_d} \right)} dz_{\text{GPS}}, \quad (2)$$

which is the differential form of Eq. (1), and corresponds to Eq. (4) in Inai et al. (2009). To avoid perturbed results from the differential equation, we calculated  $p_{\text{GPS}}$  after taking the  $\pm$ one minute running mean of the GPS height, temperature, and humidity to smooth the profile; the same smoothing was applied to Eq. (1) for consistency. Figure 2 shows the statistical feature of the pressure bias; i.e., the differences between observed pressure ( $p$ ) and GPS derived pressure ( $p_{\text{GPS}}$ ), at the same observation time from the SOWER soundings listed in Table 1.

Figure 2 shows that the RS80 pressure bias is significantly negative in the upper troposphere and stratosphere, and is  $-0.4 \pm 0.2$  hPa between 20 and 30 km. The bias is positive in the lower troposphere, but the uncertainty is large. Note that the characteristics apparent in Fig. 2 may be a restrictive result from the SOWER data, because the instrumental propensity of the RS80 could depend on the production lots to some degree. However, Stauffer et al. (2014) also reported a similar, but larger, bias ( $-1$  hPa) for the RS80 in the stratosphere than that estimated in this study. They also estimated that it is larger than that of the RS92, and is similar to the International Met Systems (iMet) series. The authors discussed the influence of pressure bias on the ozone mixing ratio, but they did not take into account an altitude offset caused by the pressure bias as pointed out by Shiotani (2013). In the following sections, errors in temperature, ozone, and water vapor profiles resulting from the RS80 pressure bias are estimated and discussed in detail.

## The impact of RS80 bias

Y. Inai et al.

Title Page

Abstract

Introduction

Conclusions

References

Tables

Figures



Back

Close

Full Screen / Esc

Printer-friendly Version

Interactive Discussion



## 4 Impact of pressure bias on observed profiles

### 4.1 Temperature

In Sect. 3, pressure bias in the RS80 was discussed on the basis of differences between observed  $p$  and  $p_{\text{GPS}}$ , and between  $z_{\text{PTU}}$  and  $z$ . As clearly shown in Fig. 1,  $z_{\text{PTU}}$  systematically differs from  $z$ , and this altitude misestimation can affect all meteorological profiles when we only have altitude information from PTU,  $z_{\text{PTU}}$ . First, we focus on the temperature profile in this subsection.

The left panel of Fig. 3 shows two temperature profiles:  $T(z_{\text{PTU}})$  (blue dashed line) and  $T(z)$  (red line), along the vertical coordinates of  $z_{\text{PTU}}$  and  $z$ , respectively. The original profile using  $z_{\text{PTU}}$  lies on the upper side of the corrected profile based on  $z$ , because there is a positive offset as seen in Fig. 1. To calculate differences between  $T(z_{\text{PTU}})$  and  $T(z)$  on the geometric altitude ( $z$ ), we need data points for  $T(z)$  and  $T(z_{\text{PTU}})$  at the same altitude, because the observation time at the same  $z$  and  $z_{\text{PTU}}$  is different. Thus, we map  $T(z_{\text{PTU}})$  on the  $z$  coordinate so as to define  $T_{\text{PTU}}(z)$  by using  $z$  in place of  $z_{\text{PTU}}$  ( $T_{\text{PTU}}(z) \equiv T(z_{\text{PTU}})$ ).

The difference  $\delta T(z)$  ( $\equiv T_{\text{PTU}}(z) - T(z)$ ) is shown in the right panel of Fig. 3. Because of the vertical shift, we usually see negative values in the stratosphere where temperature increases with increasing height. At around 30 km, an altitude offset of 230 m can produce a negative temperature bias of about  $-1.2$  K. This temperature bias is easily confirmed as the vertical gradient of temperature ( $5.0 \text{ K km}^{-1}$  in this case) multiplied by the vertical shift (0.23 km in this case). We also see some fluctuations in the temperature differences associated with gravity waves and/or equatorial waves.

Figure 4 shows an average temperature bias; i.e., the average difference of the two temperature profiles,  $T_{\text{PTU}}(z)$  and  $T(z)$  for all available soundings listed in Table 1. In the stratosphere, the temperature bias tends to increase with increasing altitude, and it is approximately  $-0.2 \pm 0.2$ ,  $-0.2 \pm 0.4$ , and  $-0.3 \pm 0.8$  K ( $1\sigma$ ) at 20, 25, and 30 km, respectively.

## The impact of RS80 bias

Y. Inai et al.

Title Page

Abstract

Introduction

Conclusions

References

Tables

Figures



Back

Close

Full Screen / Esc

Printer-friendly Version

Interactive Discussion



## 4.2 Ozone

The vertical shift of the height coordinate caused by the RS80 pressure bias can also affect other observation parameters. The ECC ozonesonde reports ozone partial pressure as its measurement principle (e.g., Johnson et al., 2002). The left panel of Fig. 5 shows two vertical profiles of ozone partial pressure, one using  $z_{\text{PTU}}$  ( $\rho\text{O}_3(z_{\text{PTU}}) \equiv \rho\text{O}_{3\text{PTU}}(z)$ ) and the other  $z$  ( $\rho\text{O}_3(z)$ ), as for Fig. 3. The profiles are taken from the same sounding as shown in Fig. 3. In the tropical region, ozone partial pressure has a maximum at approximately 27 km; consequently, the vertical gradient changes from positive to negative at around this level with increasing height.

As the ozone mixing ratio ( $\chi\text{O}_3$ ) is obtained by dividing ozone partial pressure by atmospheric pressure, the atmospheric pressure bias can lead to an error in the ozone mixing ratio. This effect has already been discussed by Stauffer et al. (2014), based on the following definition of the ozone mixing ratio error ( $\delta\chi\text{O}_3$ ):

$$\delta\chi\text{O}_3(z) = \frac{\chi\text{O}_3(z_{\text{PTU}}) - \chi\text{O}_3(z)}{\chi\text{O}_3(z)}, \quad (3)$$

where  $\chi\text{O}_3(z_{\text{PTU}})$  and  $\chi\text{O}_3(z)$  are  $\rho\text{O}_3(z_{\text{PTU}})/p(z_{\text{PTU}})$  and  $\rho\text{O}_3(z)/p_{\text{GPS}}(z)$ , respectively. Note that Stauffer et al. (2014) used these ozone partial pressures and atmospheric pressures at the same observation time. However, as we have already explained, there is a difference between  $z_{\text{PTU}}$  and  $z$ , and the mixing ratio error ( $\delta\chi\text{O}_3$ ) should be examined at the same altitude.

The middle panel of Fig. 5 is the same profile as in the left panel, but for the ozone mixing ratio. The mixing ratio error can be estimated as the difference between the original mixing ratio based on  $z_{\text{PTU}}$  ( $\chi\text{O}_3(z_{\text{PTU}}) \equiv \chi\text{O}_{3\text{PTU}}(z)$ ; blue dashed line) and the mixing ratio based on  $z$  ( $\chi\text{O}_3(z)$ ; red line) at the same altitude. As  $\chi\text{O}_{3\text{PTU}}(z) \equiv \rho\text{O}_{3\text{PTU}}(z)/p(z)$ , Eq. (3) should be replaced by the following equation:

$$\delta\chi\text{O}_3(z) = \frac{\chi\text{O}_{3\text{PTU}}(z) - \chi\text{O}_3(z)}{\chi\text{O}_3(z)}, \quad (4)$$

### The impact of RS80 bias

Y. Inai et al.

Title Page

Abstract

Introduction

Conclusions

References

Tables

Figures



Back

Close

Full Screen / Esc

Printer-friendly Version

Interactive Discussion



$$= \frac{\frac{\rho_{O_3PTU}(z)}{\rho(z)} - \frac{\rho_{O_3}(z)}{\rho_{GPS}(z)}}{\frac{\rho_{O_3}(z)}{\rho_{GPS}(z)}}. \quad (5)$$

As  $\rho(z)$  is equal to  $\rho_{GPS}(z)$  at the same level, we can replace it with  $\rho_{GPS}(z)$ ; therefore, we now have the following equation for the ozone mixing ratio error:

$$\delta\chi_{O_3}(z) = \frac{\rho_{O_3PTU}(z) - \rho_{O_3}(z)}{\rho_{O_3}(z)}. \quad (6)$$

5 As Eq. (6) is equivalent to a percentage difference in ozone partial pressure ( $\delta\rho_{O_3}$ ), we can conclude that  $\delta\chi_{O_3}(z)$  is equal to  $\delta\rho_{O_3}(z)$  and we simply write the two as  $\delta O_3$ . The right panel of Fig. 5 shows such a percentage difference for  $\delta O_3(z)$ . As expected from the left panel, it changes sign at around 27 km.

Figure 6 shows an average percentage difference calculated from all available soundings. Although the bias is small in the troposphere, it becomes larger in the lower stratosphere with a negative peak at around 20 km. At around 27 km, where there is a maximum of ozone partial pressure, the sign of ozone bias changes. There, the ozone bias is estimated to be  $-1.9 \pm 1.6$ ,  $-0.7 \pm 1.0$ , and  $3.1 \pm 2.2\%$  ( $1\sigma$ ) at 20, 25, and 30 km, respectively.

15 Stauffer et al. (2014) found that the pressure bias of the RS80 was  $-1$  hPa, which is somewhat larger than ours, as was their resulting ozone mixing ratio bias, which exponentially increases with increasing altitude. According to Fig. 7 in their paper, the ozone mixing ratio bias was approximately 2, 5, and 10 % at 20, 25, and 30 km, respectively. These estimates are based on  $\rho_{GPS}$  derived from the coincident GPS altitude. However, we estimated the RS80 pressure bias in such a case to be  $-0.4$  hPa, and the subsequent ozone bias to be negative ( $-1$  to  $-2\%$ ) at around 20–25 km, but positive (3%) at 30 km, which is not an exponential increase with increasing altitude.

Shiotani (2013) argued that what we really need to know as ozonesonde users is the difference between the true profile obtained using a GPS sensor and the observed

## The impact of RS80 bias

Y. Inai et al.

Title Page

Abstract

Introduction

Conclusions

References

Tables

Figures



Back

Close

Full Screen / Esc

Printer-friendly Version

Interactive Discussion



profile obtained using a conventional pressure sensor. However, the result in Stauffer et al. (2014) applies only to those cases where we can use coincident ozone data with pressure information derived from the GPS height to calculate the ozone mixing ratios correctly.

### 4.3 Water vapor

Profiles of water vapor in the stratosphere are observed using a chilled-mirror hygrometer that measures the frostpoint temperature as its measurement principle (e.g., Vömel et al., 2007). A profile of water vapor partial pressure and mixing ratio can be estimated from the frostpoint temperature using the Goff–Gratch equation (Goff and Gratch, 1946; List, 1984). In the SOWER campaign, water vapor profiles for the tropical lower stratosphere, as well as the troposphere, were observed using such chilled-mirror hygrometers.

A vertical profile of water vapor partial pressure based on  $z_{PTU}$  ( $\rho_{H_2O}(z_{PTU}) \equiv \rho_{H_2O_{PTU}}(z)$ ; blue dashed line) and a profile based on  $z$  ( $\rho_{H_2O}(z)$ ; red line) are shown in the left panel of Fig. 7. The water vapor mixing ratio is obtained by dividing partial pressure by atmospheric pressure ( $\chi_{H_2O} \equiv \rho_{H_2O}/p$ ); two profiles based on  $z_{PTU}$  ( $\chi_{H_2O}(z_{PTU}) \equiv \chi_{H_2O_{PTU}}(z)$ ) and  $z$  ( $\chi_{H_2O}(z)$ ) are shown in the middle panel. As for ozone, because the percentage difference in partial pressure ( $\delta\rho_{H_2O}$ ) and that of the mixing ratio ( $\delta\chi_{H_2O}$ ) become equivalent at the same altitude (see Eqs. 3–6), we simply write the two as  $\delta H_2O$ , and such a percentage difference is shown in the right panel of Fig. 7.

As is well known, the water vapor profile in the tropical lower stratosphere has a “tape recorder” signal (Mote et al., 1996; Fujiwara et al., 2010), and we can see such a signal in the vertical structure of the water vapor mixing ratio profile in Fig. 7, with the minimum at around 18 km, the maximum at around 20.5 km, and a weaker minimum at around 22 km. This vertical structure is similar to those profiles measured at Costa Rica in December-January-February 2008 shown in Fig. 3 of Fujiwara et al. (2010). As their observation period was two years earlier than that of the BI048 observations,

## The impact of RS80 bias

Y. Inai et al.

Title Page

Abstract

Introduction

Conclusions

References

Tables

Figures



Back

Close

Full Screen / Esc

Printer-friendly Version

Interactive Discussion



the two periods should be in a similar phase of the stratospheric quasi-biennial oscillation (QBO). The water vapor partial pressure profile also has a vertical structure corresponding to that of the mixing ratio, and  $\delta H_2O$  changes sign associated with the water vapor maximum at 20.5 km, as shown in the right panel.

5 An average percentage difference for water vapor calculated from all available soundings is shown in Fig. 8. The average error in the water vapor profiles was estimated to be  $-1.1 \pm 6.2\%$  at 19 km and  $1.4 \pm 0.9\%$  ( $1 \sigma$ ) at 21 km associated with the tape recorder signal. The altitudes of the cold point tropopause (CPT) and water vapor minima near the CPT vary seasonally and interannually. To focus on biases near the CPT, where the water vapor profiles have a steep gradient and minimum, we aligned the water vapor profiles according to the water vapor minimum. Figure 9 shows the average error based on relative altitude with reference to that of the water vapor minimum around the CPT. We can see that the bias is clearer than that in Fig. 8, and is estimated to be  $-2.7 \pm 8.1\%$  at 0.5 km and  $1.5 \pm 1.0\%$  ( $1\sigma$ ) at 4 km above the water vapor minimum. As there is a negative and steep gradient of water vapor abundance in the upper troposphere, a small positive error of  $Z_{PTU}$  produces a positive water vapor error at around 16 km in Fig. 8, and also below the water vapor minimum in Fig. 9. We note here that this result is based on limited soundings obtained during the boreal winter and that the vertical distribution of water vapor error in the stratosphere may differ somewhat from this result depending on the phase of the tape recorder signal.

## 5 Discussion

As described above, the RS80 pressure bias leads to temperature, ozone, and water vapor biases. If we assume that RS80 radiosondes without a GPS sensor were switched to new radiosondes with a GPS sensor during the period 2000–2010, we would expect to see such biases in the meteorological parameters that may affect any trend analysis that covers this period. In this section, we discuss issues related to long-

## The impact of RS80 bias

Y. Inai et al.

Title Page

Abstract

Introduction

Conclusions

References

Tables

Figures



Back

Close

Full Screen / Esc

Printer-friendly Version

Interactive Discussion



term trends in temperature, ozone, and water vapor, together with the possible impacts on these trends of biases associated with altitude misestimation.

Ladstädter et al. (2011) estimated temperature trends from satellite, sonde, and GPS radio occultation (RO) data between 2001 and 2010. This includes the period when the RS80 was progressively replaced by the new radiosonde system. They reported warming trends from 13 to 25 km over the tropics, as well as whole latitude region, and that the trend obtained from sonde measurements was  $0.2 \text{ Kdec}^{-1}$  higher than that obtained from satellite observations. The altitude range for their trend analysis included both the troposphere and the stratosphere, as they focused on a comparison with satellite data having a coarse vertical resolution. The discrepancy between the trends based on the sonde and satellite measurements can be interpreted to be caused by the RS80 temperature bias estimated in this study, as it is consistent with the value ( $+0.2 \text{ K}$ ) averaged over 13–25 km from Fig. 3. At the same time, however, Ladstädter et al. (2011) reported a comparable trend from GPS RO measurements to that from sonde measurements. These temperature trends should be estimated as a function of altitude and be compared in the troposphere and the stratosphere separately.

Temporal–spatial variation in the stratospheric ozone concentration is affected by ozone-depleting substances, as well as global climate change. Chemistry–climate models (CCMs) have been used to investigate these impacts on the stratospheric environment. For example, based on CCM calculations, Akiyoshi et al. (2010) suggested that there were ozone increases related to the halogen decrease during the period 2000–2100 and that the increase in the upper stratosphere is enhanced by the stratospheric cooling. On the other hand, in the tropical upper troposphere/lower stratosphere, negative ozone trends were estimated during the same period because of enhanced tropical upward motion of the residual mean circulation.

Randel and Thompson (2011) reported that the ozone mixing ratio follows a negative trend of  $-4$  and  $-0.5 \text{ \%dec}^{-1}$  in the stratosphere from 17 to 23 km and from 23 to 30 km, respectively, based on measurements from the Stratospheric Aerosol and Gas Experiment II (SAGE II) satellite (1984 to 2005) and the Southern Hemisphere

## The impact of RS80 bias

Y. Inai et al.

Title Page

Abstract

Introduction

Conclusions

References

Tables

Figures



Back

Close

Full Screen / Esc

Printer-friendly Version

Interactive Discussion



## The impact of RS80 bias

Y. Inai et al.

Title Page

Abstract

Introduction

Conclusions

References

Tables

Figures



Back

Close

Full Screen / Esc

Printer-friendly Version

Interactive Discussion



Additional Ozonesondes (SHADOZ) network (1998 to 2009). They pointed out that the negative trends in the lower stratosphere are a dynamical response to enhanced tropical upwelling. On the other hand, Gabhardt et al. (2014) reported positive trends in the same altitude region based on SCanning Imaging Absorption spectroMeter for Atmospheric CHartographY (SCIAMACHY) satellite measurements (2002 to 2012). In particular, they argued that the positive trend between 25 and 30 km cannot be explained in terms of enhanced tropical upwelling.

As discussed above, a switch from the RS80 to the new GPS radiosondes may create an artificial ozone trend; i.e., a positive trend of 1 to 2 % at around 20 km, and a negative trend of −3 % at 30 km. It is possible that the negative trend is larger than that estimated by Randel and Thompson (2011) in view of the present results. Gabhardt et al. (2014) mentioned the need to consider both changing dynamics and chemical composition to explain the positive trend, such as an increase in NO<sub>x</sub>, resulting in an ozone enhancement in the tropical stratosphere (Nevison et al., 1999). Moreover, an issue exists regarding the sensor response time of the ECC ozonesonde (~ 30 s), resulting in an ozone bias of more than −5 % in the tropics (Imai et al., 2013).

In addition to the annual variations reflected in the tape recorder signal, water vapor abundance in the upper troposphere and lower stratosphere shows interannual variations depending on the El Niño–Southern Oscillation (ENSO) and the QBO (e.g., Randel et al., 2004). For longer-term variations, Hurst et al. (2011) reported that water vapor in the mid-latitude lower stratosphere from 16 to 26 km decreased during the period 2001–2005 by an average of 0.4 ppmv, then increased again during the period 2006–2010 by an average of 0.5 ppmv. As for temperature and ozone, the water vapor bias caused by the altitude misestimation affects these water vapor observation records, and the biases are estimated to be approximately −3 to 1.5 %, depending on altitude, in the lower stratosphere.

Whereas the water vapor bias is smaller than its stratospheric trend, those for temperature and ozone are comparable in magnitude to their decadal trends in the lower

stratosphere. Therefore, these long-term variations should be discussed after examining and correcting these radiosonde errors.

## 6 Summary

At present, GPS technology is used to measure altitude, and pressure is inversely derived from the GPS height data. Although the Vaisala RS80 radiosonde was used worldwide from 1981, such old-type radiosondes without a GPS receiver have been replaced by new-type radiosondes with a GPS receiver over the past decade. Recently, it has been reported that the RS80 radiosonde shows a negative pressure bias in the stratosphere (e.g., Steinbrecht et al., 2008; Inai et al., 2009).

In this study, we estimated that the pressure bias in the tropical stratosphere, as assessed using the SOWER dataset for the period from December 2003 to January 2010, is  $-0.4 \pm 0.2$  hPa ( $1\sigma$ ) from 20 to 30 km. We also estimated that this pressure bias could lead to an altitude misestimation of  $42 \pm 24$ ,  $110 \pm 39$ , and  $240 \pm 90$  m ( $1\sigma$ ) at 20, 25, and 30 km, respectively.

This altitude misestimation can lead to biases in other meteorological profiles, such as temperature, ozone, and water vapor. We found that in the stratosphere the temperature bias caused by such altitude misestimation tends to increase with increasing altitude, and it is approximately  $-0.2 \pm 0.2$ ,  $-0.2 \pm 0.4$ , and  $-0.3 \pm 0.8$  K ( $1\sigma$ ) at 20, 25, and 30 km, respectively. On the other hand, for the ozone bias its sign changes at 27 km where there is a maximum of ozone partial pressure, and it is estimated to be  $-1.9 \pm 1.6$ ,  $-0.7 \pm 1.0$ , and  $3.1 \pm 2.2$  % ( $1\sigma$ ) at 20, 25, and 30 km, respectively. For water vapor, there is a minimum and maximum in the tropical lower stratosphere associated with the tape recorder signal. Thus, the water vapor bias is affected by the phase of the tape recorder and is estimated to be  $-2.7 \pm 8.1$  % at 0.5 km and  $1.5 \pm 1.0$  % ( $1\sigma$ ) at 4 km above the water vapor minimum around the cold point tropopause.

These temperature, ozone, and water vapor biases may produce an artificial change in long-term meteorological records at the time when the radiosonde system changed

## The impact of RS80 bias

Y. Inai et al.

Title Page

Abstract

Introduction

Conclusions

References

Tables

Figures



Back

Close

Full Screen / Esc

Printer-friendly Version

Interactive Discussion



from the RS80 to the new model. Therefore, we must take these issues into account if we are to compile accurate meteorological datasets and improve our understanding of climate change.

## Appendix A

5 Here, we describe how we processed the original pressure profiles prior to analysis. Each pressure sensor in the RS80 radiosondes has its own uncertainty, in addition to the pressure bias described in this paper. If we plot the differences between  $Z_{PTU}$  and  $z$ , similar to Fig. 1 but using uncorrected (original) profiles, the result is as in Fig. 10. We see larger variability of profiles in this figure than in Fig. 1, because original  
10 pressure information sometimes includes a large error. To reduce this variation, we made a correction by using a constant offset value for the entire height range. The correction value was subjectively determined to fit a profile to the average. A frequency distribution of the correction values for pressure offset is shown in Fig. 11. On the basis of these statistics, we excluded five profiles using the criterion that the absolute value  
15 of the pressure offset should not be larger than 1.5 hPa, and so used 33 soundings (out of a total of 38) in this study.

*Acknowledgements.* The authors are grateful to SOWER colleagues, K. Shimizu, S.-Y. Ogino, S. Iwasaki, N. Nishi, and T. Shibata for their assistance. We also thank the members of Lembaga Penerbangan dan Antariksa Nasional (LAPAN) of Indonesia, and the Meteorological Of-  
20 fice of Tarawa, Kiribati. This work was supported by KAKENHI, Japan Society for the Promotion of Science, Japan (15204043, 16740264, 18204041, and 21244072), and the Global Environment Research Fund of the Ministry of the Environment (A-1 and A-071). The figures were produced by the GFD-DENNOU Library.

## The impact of RS80 bias

Y. Inai et al.

Title Page

Abstract

Introduction

Conclusions

References

Tables

Figures



Back

Close

Full Screen / Esc

Printer-friendly Version

Interactive Discussion



## References

- Akiyoshi, H., Yamashita, Y., Sakamoto, K., Zhou, L. B., and Imamura, T.: Recovery of stratospheric ozone in calculations by the Center for Climate System Research/National Institute for Environmental Studies chemistry-climate model under the CCMVal-REF2 scenario and a no-climate-change run, *J. Geophys. Res.*, 115, D19301, doi:10.1029/2009JD012683, 2010. 2203
- 5 da Silveira, R., Fisch, G., Machado, L., Dall'Antonia, A., Sapucci, L., Fernandes, D., and Marques, R.: WMO intercomparison of GPS radiosondes, Alcantara, Brazil, 2001, WMO/TD No. 1314, Instruments and Observing Methods Report No. 90, World Meteorological Organization, Geneva, 65 pp., 2006. 2193
- 10 Elms, J.: WMO catalogue of radiosondes and upper-air wind systems in use by members in 2002 and compatibility of radiosonde geopotential measurements for period from 1998 to 2001, Report No. 80, WMO/TD No. 1197, World Meteorological Organization, Geneva, 2003. 2193
- 15 Fujiwara, M., Vömel, H., Hasebe, F., Shiotani, M., Ogino, S.-Y., Iwasaki, S., Nishi, N., Shibata, T., Shimizu, K., Nishimoto, E., Canossa, J. M. V., Selkirk, H. B., and Oltmans, S. J.: Seasonal to decadal variations of water vapor in the tropical lower stratosphere observed with balloon-borne cryogenic frost point hygrometers, *J. Geophys. Res.*, 115, D18304, doi:10.1029/2010JD014179, 2010. 2195, 2201
- 20 Gebhardt, C., Rozanov, A., Hommel, R., Weber, M., Bovensmann, H., Burrows, J. P., Densten, D., Froidevaux, L., and Thompson, A. M.: Stratospheric ozone trends and variability as seen by SCIAMACHY from 2002 to 2012, *Atmos. Chem. Phys.*, 14, 831–846, doi:10.5194/acp-14-831-2014, 2014. 2204
- Goff, A. J. and Gratch, S.: Low-pressure properties of water from –160 to 212 °F, *Trans. Amer. Soc. Heat. Vent. Eng.*, 52, 95–122, 1946. 2201
- 25 Hasebe, F., Inai, Y., Shiotani, M., Fujiwara, M., Vömel, H., Nishi, N., Ogino, S.-Y., Shibata, T., Iwasaki, S., Komala, N., Peter, T., and Oltmans, S. J.: Cold trap dehydration in the Tropical Tropopause Layer characterised by SOWER chilled-mirror hygrometer network data in the Tropical Pacific, *Atmos. Chem. Phys.*, 13, 4393–4411, doi:10.5194/acp-13-4393-2013, 2013. 2195
- 30 Holton, J. R.: *An Introduction to Dynamic Meteorology*, 4th Edn., Elsevier Academic Press, New York, 535 pp., 2004. 2196

## The impact of RS80 bias

Y. Inai et al.

Title Page

Abstract

Introduction

Conclusions

References

Tables

Figures



Back

Close

Full Screen / Esc

Printer-friendly Version

Interactive Discussion



- Hurst, D. F., Oltmans, S. J., Vömel, H., Rosenlof, K. H., Sean, M. Davis, S. M., Ray, E. A., Hall, E. G., and Jordan, A. F.: Stratospheric water vapor trends over Boulder, Colorado: analysis of the 30 year Boulder record, *J. Geophys. Res.*, 116, D02306, doi:10.1029/2010JD01506510.1029/2010JD015065, 2011. 2204
- 5 Imai, K., Fujiwara, M., Inai, Y., Manago, N., Suzuki, M., Sano, T., Mitsuda, C., Naito, Y., Hasebe, F., Koide, T., and Shiotani, M.: Comparison of ozone profiles between Superconducting Submillimeter-Wave Limb-Emission Sounder (SMILES) and worldwide ozonesonde measurements, *J. Geophys. Res.-Atmos.*, 118, 12755–12765, doi:10.1002/2013JD021094, 2013. 2195, 2204
- 10 Inai, Y., Hasebe, F., Shimizu, K., and Fujiwara, M.: Correction of radiosonde pressure and temperature measurements using simultaneous GPS height data, *SOLA*, 5, 109–112, doi:10.2151/sola.2009-02810.2151/sola.2009-028, 2009. 2193, 2195, 2196, 2197, 2205
- Inai, Y., Shibata, T., Fujiwara, M., Hasebe, F., and Vömel, H.: High supersaturation inside cirrus in well-developed tropical tropopause layer over Indonesia, *Geophys. Res. Lett.*, 39, L20811, doi:10.1029/2012GL05363810.1029/2012GL053638, 2012. 2195
- 15 Inai, Y., Hasebe, F., Fujiwara, M., Shiotani, M., Nishi, N., Ogino, S.-Y., Vömel, H., Iwasaki, S., and Shibata, T.: Dehydration in the tropical tropopause layer estimated from the water vapor match, *Atmos. Chem. Phys.*, 13, 8623–8642, doi:10.5194/acp-13-8623-2013, 2013. 2195
- Ivanov, A., Kats, A., Kurnosenko, S., Nash, J., and Zaitseva, N.: WMO international radiosonde intercomparison phase III (Dzhambul, USSR, 1989) final report (WMO/TD-451), *Instrum., and Observ. Methods Rep. 40*, World Meteorological Organization, Geneva, 135 pp., 1991. 2193
- 20 Jeannot, P., Bower, C., and Calpini, B.: Global Criteria for Tracing the Improvements of Radiosondes over the Last Decades Instruments and Observing Methods, Report No. 95, WMO/TD No. 1433, World Meteorological Organization, Geneva, 2008. 2193
- 25 Johnson, B. J., Oltmans, S. J., Vömel, H., Smit, H. G. J., Deshler, T., and Kroger, C.: Electrochemical concentration cell (ECC) ozonesonde pump efficiency measurements and tests on the sensitivity to ozone of buffered and unbuffered ECC sensor cathode solutions, *J. Geophys. Res.*, 107, 4393, doi:10.1029/2001JD000557, 2002. 2199
- 30 Ladstädter, F., Steiner, A. K., Foelsche, U., Haimberger, L., Tavolato, C., and Kirchengast, G.: An assessment of differences in lower stratospheric temperature records from (A)MSU, radiosondes, and GPS radio occultation, *Atmos. Meas. Tech.*, 4, 1965–1977, doi:10.5194/amt-4-1965-2011, 2011. 2194, 2203

## The impact of RS80 bias

Y. Inai et al.

Title Page

Abstract

Introduction

Conclusions

References

Tables

Figures

◀

▶

◀

▶

Back

Close

Full Screen / Esc

Printer-friendly Version

Interactive Discussion



- List, R. J.: Smithsonian Meteorological Tables, 5th Edn., Smithsonian Institution, Washington, DC, 1984. 2201
- Mahoney, M.: A Discussion of Various Measures of Altitude, Tech. rep., NASA Jet Propulsion Laboratory, 2005. 2196
- 5 Mote, P. W., Rosenlof, K. H., McIntyre, M. E., Carr, E. S., Gille, J. C., Holton, J. R., Kinnerley, J. S., Pumphrey, H. C., Russell III, J. M., and Waters, J. W.: An atmospheric tape recorder: the imprint of tropical tropopause temperatures on stratospheric water vapor, *J. Geophys. Res.*, 101, 3989–4006, 1996. 2201
- NIMA (National Imagery and Mapping Agency): Department of Defence World Geodetic System 1984 – Its Definition and Relationships with Local Geodetic Systems, NIMA Technical Report, NIMA TR8350.2, 3rd Edn., Amendment 1, 3 January 2000. 2195, 2196
- 10 Nash, J. and Schmidlin, F. J.: WMO international radiosonde comparison (UK 1984, USA 1985), Final Report, WMO Instruments and Observing Methods, Report No. 30, WMO/TD-No. 195, Word Meteorol. Org., Geneva, viii +103 pp., 1987. 2193
- 15 Nash, J., Smout, R., Oakley, T., Pathack, B., and Kurnosenko, S.: WMO intercomparison of radiosonde systems, Vacoas, Mauritius, 2–25 February 2005, WMO/TD-No. 1303, 115 pp., 2006. 2193, 2196
- Nash, J., Oakley, T., Vömel, H., and Wei, L.: WMO intercomparison of high quality radiosonde systems, Yangjiang, China, 12 July–3 August 2010, WMO/TD-No. 1580, 248 pp., available at: <http://www.wmo.int/pages/prog/www/IMOP/publications-IOM-series.html>, 2011. 2193
- 20 Nevison, C. D., Solomon, S., and Gao, R. S.: Buffering interactions in the modeled response of stratospheric O<sub>3</sub> to increased NO<sub>x</sub> and HO<sub>x</sub>, *J. Geophys. Res.*, 104, 3741–3754, doi:10.1029/1998JD100018, 1999. 2204
- Randel, W. J. and Thompson, A. M.: Interannual variability and trends in tropical ozone derived from SAGE II satellite data and SHADOZ ozonesondes, *J. Geophys. Res.*, 116, D07303, doi:10.1029/2010JD015195, 2011. 2194, 2203, 2204
- 25 Randel, W. J. and Wu, F.: Biases in stratospheric and tropospheric temperature trends derived from historical radiosonde data, *J. Climate*, 19, 2094–2104, doi:10.1175/JCLI3717.1, 2006. 2193
- 30 Randel, W. J., Wu, F., Oltmans, S. J., Rosenlof, K., and Nedoluha, G. E.: Interannual changes of stratospheric water vapor and correlations with tropical tropopause temperatures, *J. Atmos. Sci.*, 61, 2133–2148, 2004. 2204

## The impact of RS80 bias

Y. Inai et al.

Title Page

Abstract

Introduction

Conclusions

References

Tables

Figures



Back

Close

Full Screen / Esc

Printer-friendly Version

Interactive Discussion



- Randel, W. J., Shine, K. P., Austin, J., Barnett, J., Claud, C., Gillett, N. P., Keckhut, P., Lange-  
matz, U., Lin, R., Long, C., Mears, C., Miller, A., Nash, J., Seidel, D. J., Thompson, D. W. J.,  
Wu, F., and Yoden, S.: An update of observed stratospheric temperature trends, *J. Geophys.*  
*Res.*, 114, D02107, doi:10.1029/2008JD010421, 2009. 2193
- 5 Shibata, T., Hayashi, M., Naganuma, A., Hara, N., Hara, K., Hasebe, F., Shimizu, K., Ko-  
mala, N., Inai, Y., Vömel, H., Hamdi, S., Iwasaki, S., Fujiwara, M., Shiotani, M., Ogino, S.-Y.,  
and Nishi, N.: Cirrus cloud appearance in a volcanic aerosol layer around the tropical cold  
point tropopause over Biak, Indonesia, in January 2011, *J. Geophys. Res.*, 117, D11209,  
doi:10.1029/2011JD017029, 2012. 2195
- 10 Shiotani, M.: *Interactive Comment on* “Propagation of radiosonde pressure sensor errors to  
ozonesonde measurements” by R. M. Stauffer et al., *Atmos. Meas. Tech. Discuss.*, 6, C2996–  
C3000, 2013. 2197, 2200
- Steinbrecht, W., Claude, H., Schönenborn, F., Leiterer, U., Dier, H., and Lanzinger, E.: Pres-  
sure and temperature differences between Vaisala RS80 and RS92 radiosonde systems, *J.*  
15 *Atmos. Ocean. Tech.*, 25, 909–927, 2008. 2193, 2205
- Stauffer, R. M., Morris, G. A., Thompson, A. M., Joseph, E., Coetzee, G. J. R., and Nalli, N. R.:  
Propagation of radiosonde pressure sensor errors to ozonesonde measurements, *Atmos.*  
*Meas. Tech.*, 7, 65–79, doi:10.5194/amt-7-65-2014, 2014. 2194, 2195, 2196, 2197, 2199,  
2200, 2201
- 20 Vömel, H., David, D., and Smith, K.: Accuracy of tropospheric and stratospheric water vapor  
measurements by the cryogenic frost point hygrometer: instrumental details and observa-  
tions, *J. Geophys. Res.*, 112, D08305, doi:10.1029/2006JD007224, 2007. 2201
- Yagi, S., Mita, A., and Inoue, N.: WMO international radiosonde intercomparison phase IV  
(Tsukuba, Japan, 1993) final report, WMO/TD No. 742, *Instruments and Observing Methods*  
25 *Report No. 59*, World Meteorological Organization, Geneva, 130 pp., 1996. 2193

## The impact of RS80 bias

Y. Inai et al.

Title Page

Abstract

Introduction

Conclusions

References

Tables

Figures



Back

Close

Full Screen / Esc

Printer-friendly Version

Interactive Discussion



**Table 1.** Number of successful soundings by the SOWER campaign between December 2003 and January 2010, and the locations of campaign sites.

Station	Location (long./lat.)	Soundings
Kototabang	(100.32° E, 0.20° S)	6
Bandung	(107.59° E, 6.89° S)	4
Biak	(136.06° E, 1.17° S)	16
Tarawa	(172.92° E, 1.35° N)	7

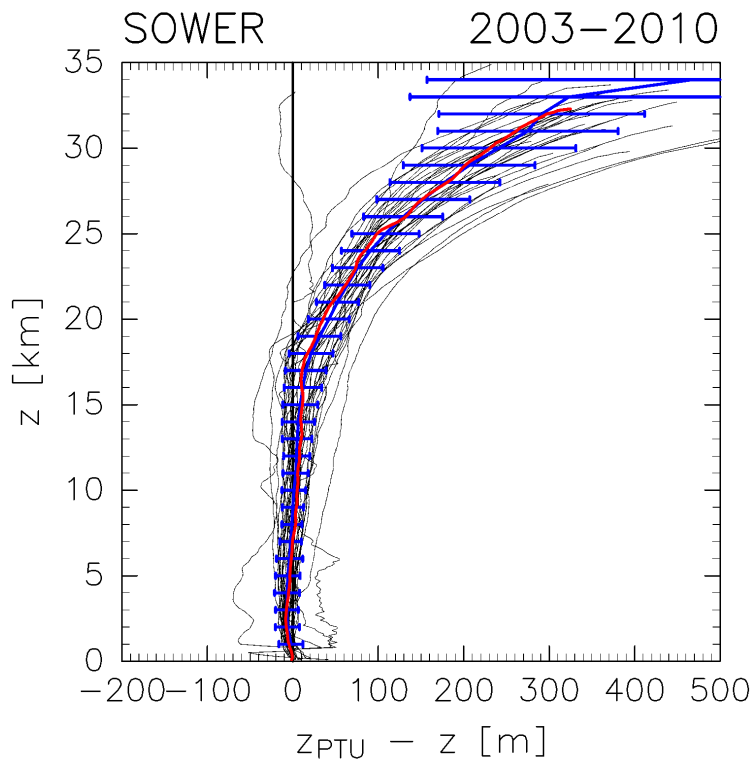


**Figure 1.** Differences between  $z_{PTU}$  and  $z$  ( $z_{PTU}$  minus  $z$ ) for all soundings in Table 1 (black lines) and for BI048 observations, which are shown in Figs. 3, 5, and 7 as an example (red line). The blue line and horizontal bars indicate the mean difference and one standard deviation calculated at each altitude, respectively.

The impact of RS80 bias

Y. Inai et al.

Title Page	
Abstract	Introduction
Conclusions	References
Tables	Figures
◀	▶
◀	▶
Back	Close
Full Screen / Esc	
Printer-friendly Version	
Interactive Discussion	



**The impact of RS80 bias**

Y. Inai et al.

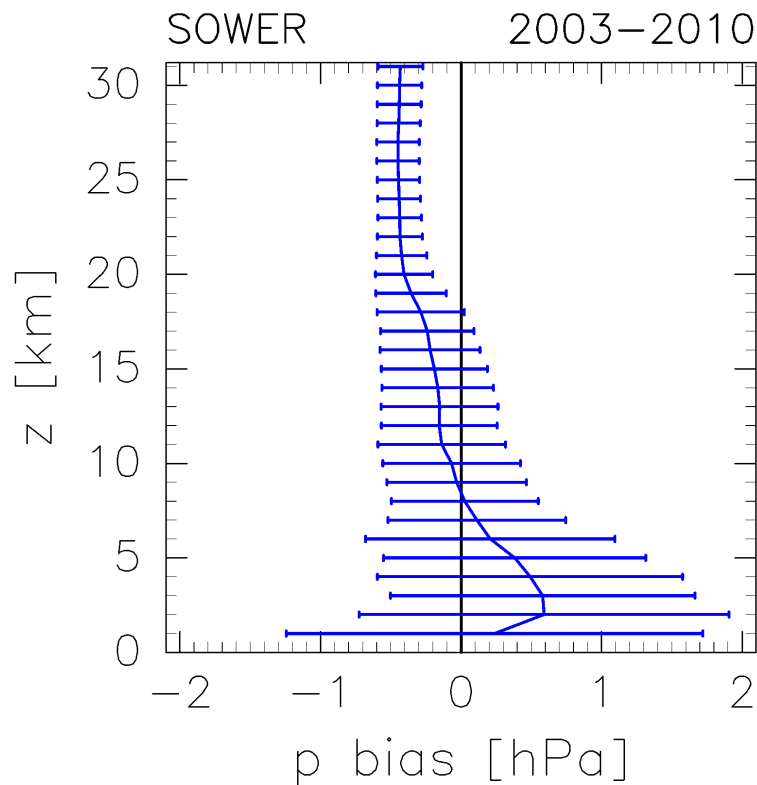


**Figure 2.** RS80 pressure bias estimated for all soundings listed in Table 1. Horizontal bars show one standard deviation.

[Title Page](#)[Abstract](#)[Introduction](#)[Conclusions](#)[References](#)[Tables](#)[Figures](#)[◀](#)[▶](#)[◀](#)[▶](#)[Back](#)[Close](#)[Full Screen / Esc](#)[Printer-friendly Version](#)[Interactive Discussion](#)

## The impact of RS80 bias

Y. Inai et al.

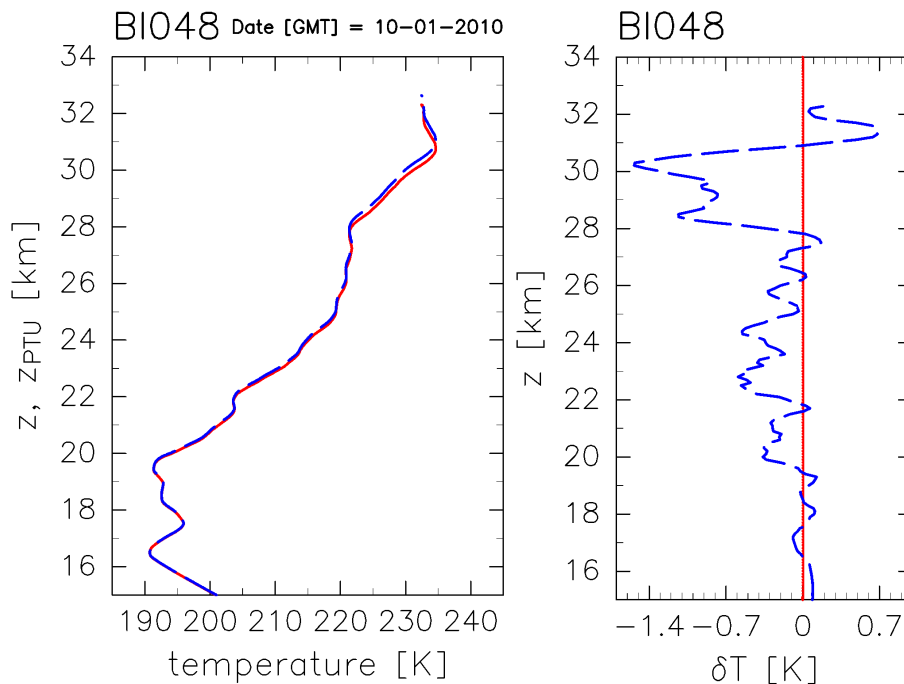


**Figure 3.** (Left) Example of temperature profiles based on  $z_{PTU}$  ( $T(z_{PTU}) \equiv T_{PTU}(z)$ ; blue dashed line) and  $z$  ( $T(z)$ ; red line) measured over Biak on 10 January 2010. (Right) Difference between the two temperature profiles in the left panel, defined as  $T_{PTU}(z)$  minus  $T(z)$  (blue dashed line).

Title Page

Abstract

Introduction

Conclusions

References

Tables

Figures

◀

▶

◀

▶

Back

Close

Full Screen / Esc

Printer-friendly Version

Interactive Discussion



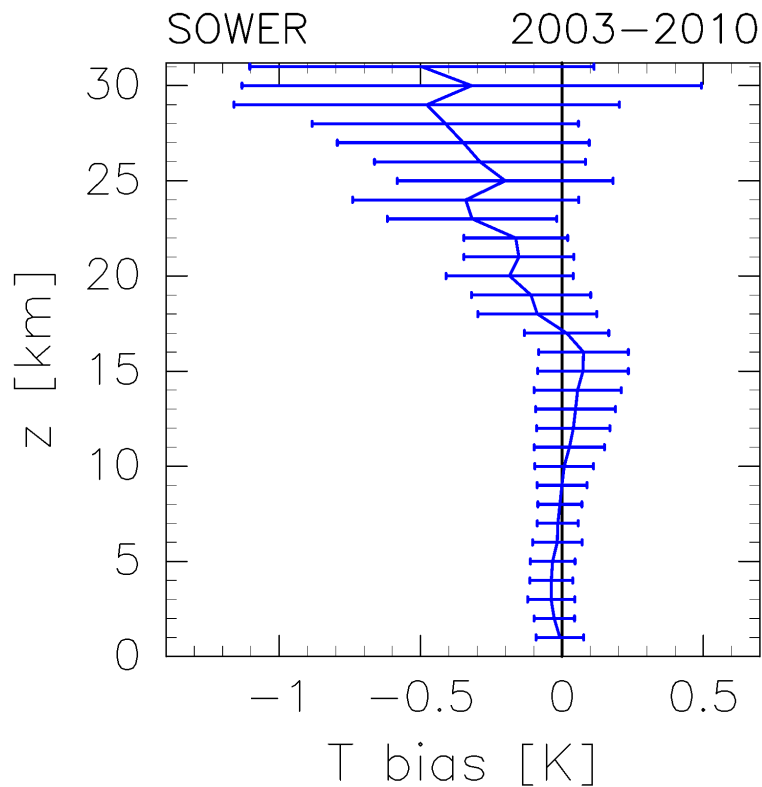


**Figure 4.** Temperature bias caused by the RS80 pressure bias via the altitude error estimated for all soundings listed in Table 1. Horizontal bars indicate one standard deviation.

**The impact of RS80 bias**

Y. Inai et al.

Title Page

Abstract

Introduction

Conclusions

References

Tables

Figures

◀

▶

◀

▶

Back

Close

Full Screen / Esc

Printer-friendly Version

Interactive Discussion



## The impact of RS80 bias

Y. Inai et al.

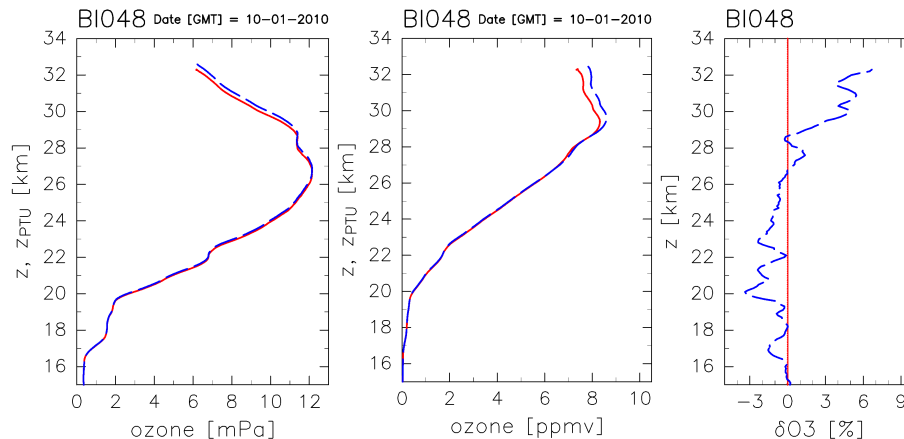


**Figure 5.** As for Fig. 3 but for (left) ozone partial pressure ( $pO_3(z_{PTU}) \equiv pO_{3PTU}(z)$ ) shown by blue dashed line and  $pO_3(z)$  by the red line) and (center) ozone mixing ratio ( $\chi O_3(z_{PTU}) \equiv \chi O_{3PTU}(z)$ ) shown by the blue dashed line, and  $\chi O_3(z)$  by the red line). (Right) Difference in the ozone profiles for partial pressure and mixing ratio ( $pO_{3PTU}(z)$  minus  $pO_3(z)$  or  $\chi O_{3PTU}(z)$  minus  $\chi O_3(z)$ ; blue dashed line).

Title Page

Abstract

Introduction

Conclusions

References

Tables

Figures

◀

▶

◀

▶

Back

Close

Full Screen / Esc

Printer-friendly Version

Interactive Discussion



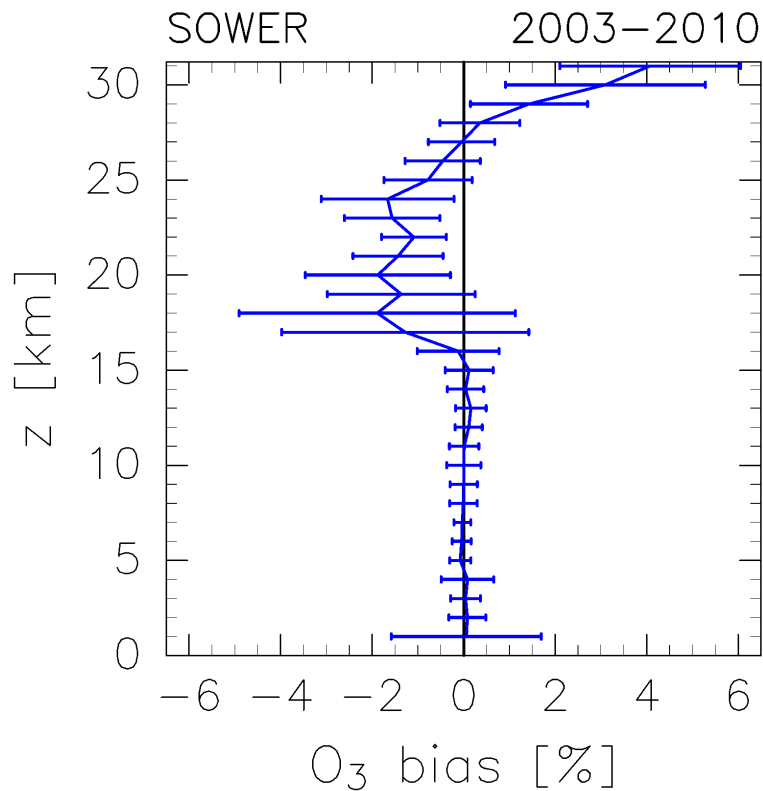


**Figure 6.** As for Fig. 4 but for ozone partial pressure and mixing ratio.

**The impact of RS80 bias**

Y. Inai et al.

Title Page

Abstract

Introduction

Conclusions

References

Tables

Figures



Back

Close

Full Screen / Esc

Printer-friendly Version

Interactive Discussion



## The impact of RS80 bias

Y. Inai et al.

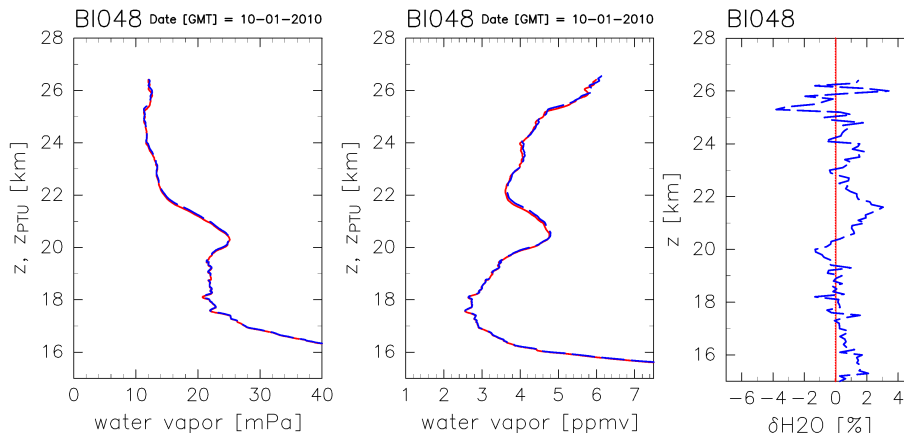


**Figure 7.** As for Fig. 3 but for (left) water vapor partial pressure ( $\rho_{\text{H}_2\text{O}}(z_{\text{PTU}}) \equiv \rho_{\text{H}_2\text{O}_{\text{PTU}}}(z)$ ) shown by the blue dashed line, and  $\rho_{\text{H}_2\text{O}}(z)$  by the red line) and (center) water vapor mixing ratio ( $\chi_{\text{H}_2\text{O}}(z_{\text{PTU}}) \equiv \chi_{\text{H}_2\text{O}_{\text{PTU}}}(z)$ ) shown by the blue dashed line, and  $\chi_{\text{H}_2\text{O}}(z)$  by the red line). (Right) Difference in the ozone profiles for partial pressure and mixing ratio ( $\rho_{\text{H}_2\text{O}_{\text{PTU}}}(z)$  minus  $\rho_{\text{H}_2\text{O}}(z)$  or  $\chi_{\text{H}_2\text{O}_{\text{PTU}}}(z)$  minus  $\chi_{\text{H}_2\text{O}}(z)$ ); blue dashed line).

Title Page

Abstract

Introduction

Conclusions

References

Tables

Figures

◀

▶

◀

▶

Back

Close

Full Screen / Esc

Printer-friendly Version

Interactive Discussion



**The impact of RS80 bias**

Y. Inai et al.

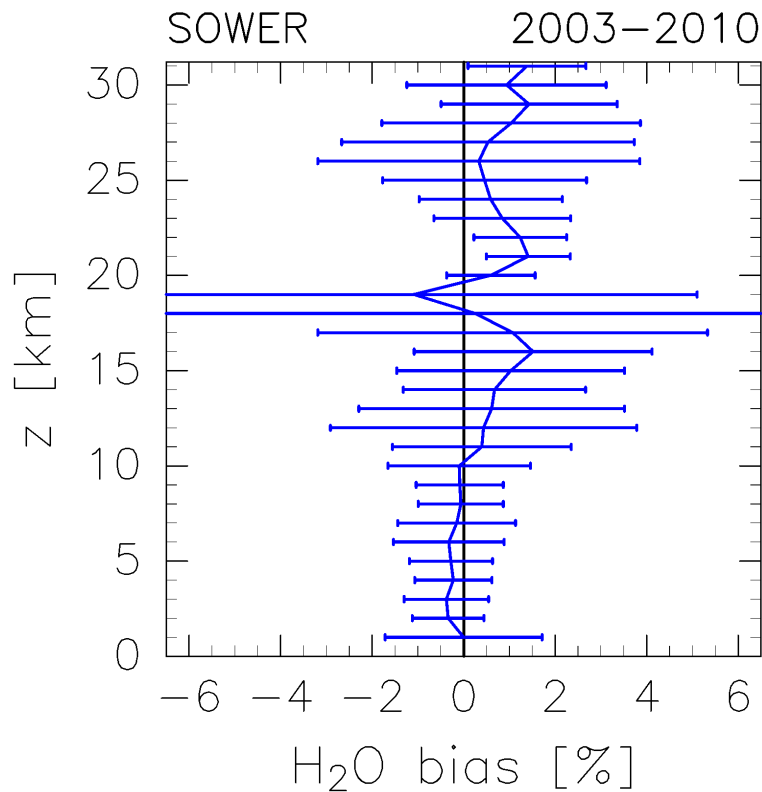


**Figure 8.** As for Fig. 4 but for water vapor partial pressure and mixing ratio.

[Title Page](#)[Abstract](#)[Introduction](#)[Conclusions](#)[References](#)[Tables](#)[Figures](#)[◀](#)[▶](#)[◀](#)[▶](#)[Back](#)[Close](#)[Full Screen / Esc](#)[Printer-friendly Version](#)[Interactive Discussion](#)

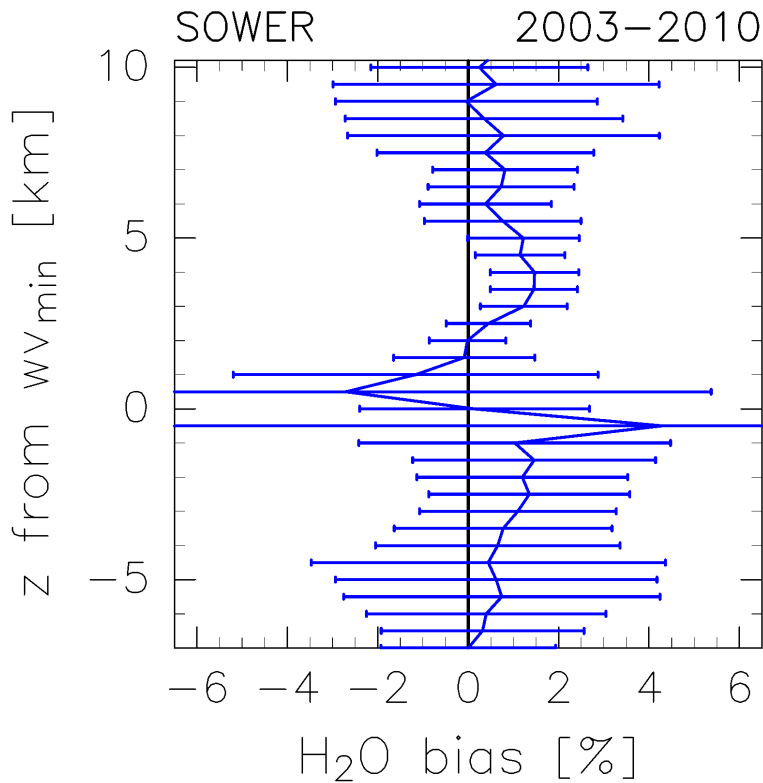


**Figure 9.** As for Fig. 8 but for the biases based on relative altitude with reference to that of the water vapor minimum near the CPT.

**The impact of RS80 bias**

Y. Inai et al.

Title Page	
Abstract	Introduction
Conclusions	References
Tables	Figures
◀	▶
◀	▶
Back	Close
Full Screen / Esc	
Printer-friendly Version	
Interactive Discussion	



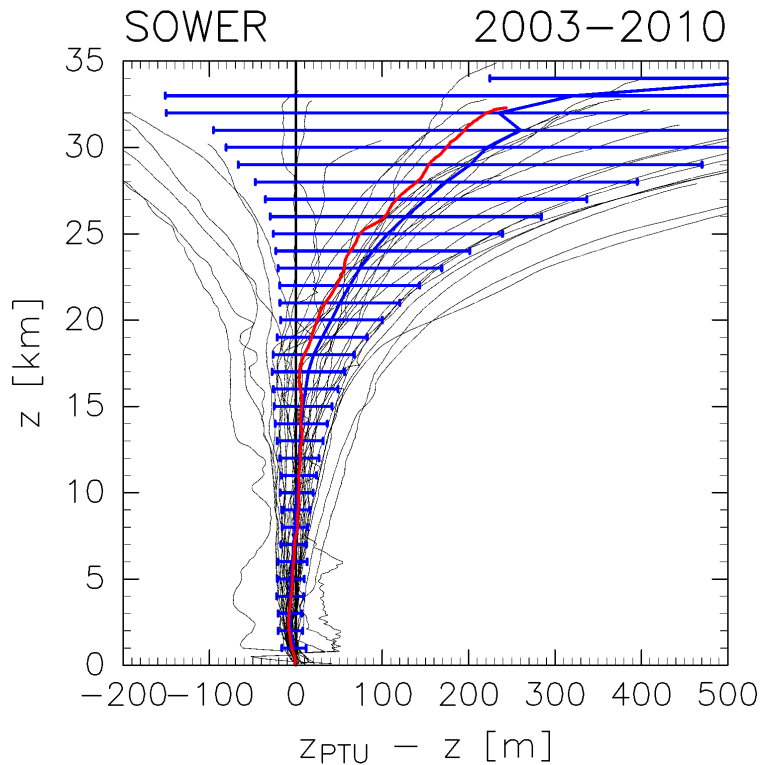


**Figure 10.** As for Fig. 1 but for profiles using non-QC data.

**The impact of RS80 bias**

Y. Inai et al.

Title Page

Abstract

Introduction

Conclusions

References

Tables

Figures



Back

Close

Full Screen / Esc

Printer-friendly Version

Interactive Discussion



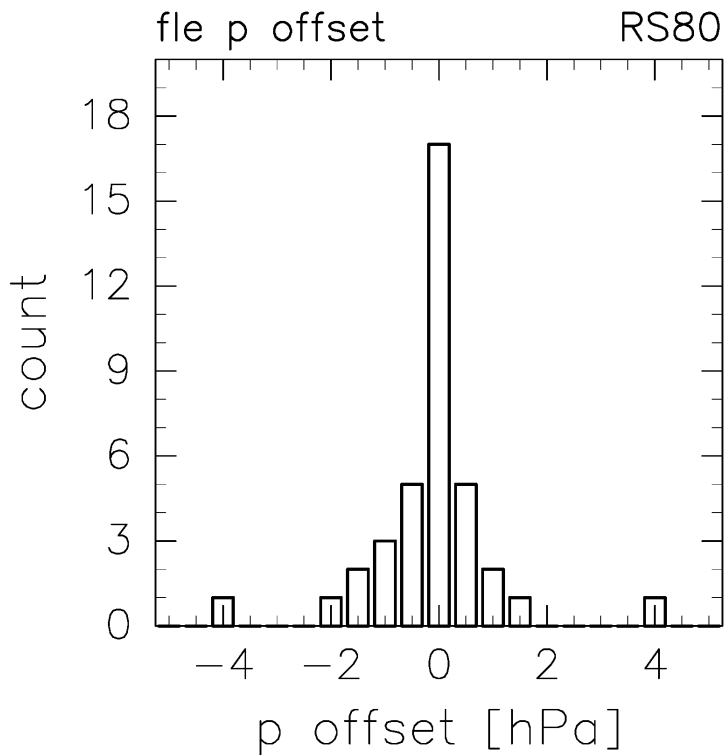


**Figure 11.** Frequency distribution of pressure offset, which was empirically determined using our QC procedure. The data are split into  $\pm 0.25$  hPa bins with an increment of 0.5 hPa and a total of 38 soundings.

**The impact of RS80 bias**

Y. Inai et al.

Title Page

Abstract Introduction

Conclusions References

Tables Figures

◀ ▶

◀ ▶

Back Close

Full Screen / Esc

Printer-friendly Version

Interactive Discussion

